electronics

MDPI

Article

Motor Fault Diagnosis and Detection with Convolutional Autoencoder (CAE) Based on Analysis of Electrical Energy Data

YuRim Choi and Inwhee Joe *

Department of Computer Science, Hanyang University, Seoul 04763, Republic of Korea; ylchoi11@hanyang.ac.kr
* Correspondence: iwjoe@hanyang.ac.kr; Tel.: +82-2-2220-1088

Abstract: This study develops a Convolutional Autoencoder (CAE) and deep neural network (DNN)-based model optimized for real-time signal processing and high accuracy in motor fault diagnosis. This model learns complex patterns from voltage and current data and precisely analyzes them in combination with DNN through latent space representation. Traditional diagnostic methods relied on vibration and current sensors, empirical knowledge, or harmonic and threshold-based monitoring, but they had limitations in recognizing complex patterns and providing accurate diagnoses. Our model significantly enhances the accuracy of power data analysis and fault diagnosis by mapping each phase (R, S, and T) of the electrical system to the red, green, and blue (RGB) channels of image processing and applying various signal processing techniques. Optimized for real-time data streaming, this model demonstrated high practicality and effectiveness in an actual industrial environment, achieving 99.9% accuracy, 99.8% recall, and 99.9% precision. Specifically, it was able to more accurately diagnose motor efficiency and fault risks by utilizing power system analysis indicators such as phase voltage, total harmonic distortion (THD), and voltage unbalance. This integrated approach significantly enhances the real-time applicability of electric motor fault diagnosis and is expected to provide a crucial foundation for various industrial applications in the future.

Keywords: motor fault diagnosis; convolutional autoencoder (CAE); deep neural network (DNN); real-time data processing; predictive maintenance; anomaly detection; energy efficiency

Citation: Choi, Y.; Joe, I. Motor Fault Diagnosis and Detection with Convolutional Autoencoder (CAE) Based on Analysis of Electrical Energy Data. *Electronics* **2024**, *13*, 3946. https://doi.org/10.3390/electronics13193946

Academic Editor: Wei Wang

Received: 18 August 2024
Revised: 19 September 2024
Accepted: 2 October 2024
Published: 7 October 2024

1. Introduction

Electric energy is essential for all electrical machinery, and globally, motors account for approximately 43–46% of the total power consumption [1]. Improving the efficiency of electric motors plays a vital role not only in enhancing economic and environmental sustainability but also in reducing energy consumption and carbon dioxide emissions [2,3]. The efficient operation of motors, particularly in industrial and manufacturing processes, is crucial for increasing productivity and reducing operational costs [4]. In this context, motor fault diagnosis has emerged as a critical technology for extending motor lifespan and preventing emergency shutdowns [5]. However, conventional studies have primarily relied on vibration signals or current signals, which have limitations in recognizing complex fault patterns [6,7]. These methods struggled to accurately identify fault types [8] and often suffered from performance degradation in real-time analysis [9].

This study proposes a novel approach that combines a Convolutional Autoencoder (CAE) with a deep neural network (DNN) to overcome the limitations of the existing methods. The proposed model learns complex patterns from voltage and current data in real time and analyzes high-dimensional features in the latent space, enabling precise fault diagnosis. Notably, the model transforms electrical energy data into an image processing format, offering a differentiated analysis framework by using power system analysis indicators—such as total harmonic distortion (THD) and voltage unbalance—for fault

diagnosis, a method not previously explored in the existing studies. This approach enables the early detection and prediction of motor faults.

Unlike traditional methodologies, this study presents a model optimized for real-time motor fault diagnosis, applicable in industrial environments. By focusing on the analysis of complex patterns in electrical energy data, the proposed model maximizes both diagnostic accuracy and speed. Furthermore, the model demonstrated 99.9% accuracy in performance comparison experiments with other machine learning models, proving its practical applicability in real-world settings.

In conclusion, this study overcomes the limitations of previous research in electric motor fault diagnosis and offers a high-precision, real-time fault diagnosis model by integrating power system analysis data with a CNN-based autoencoder and DNN. This contribution is expected to provide a foundation for various industrial applications in the future.

Figure 1 summarizes the data processing and analysis procedure for motor fault diagnosis. In Figure (a) data collection, voltage and current data from the motor are collected. In Figure (b) real-time data processing and analysis, the data are processed in real time using a power system analyzer, and if any abnormal signs are detected, the data are transmitted. Figure (c) time-series data segmentation through the sliding window technique involves segmenting the data into frames to extract significant features. Finally, in Figure (d) fault prediction through the combined CAE + DNN model, the extracted features are utilized to accurately predict motor faults. This integrated approach enhances the accuracy of motor fault diagnosis and improves upon the existing methods by enabling real-time applicability.

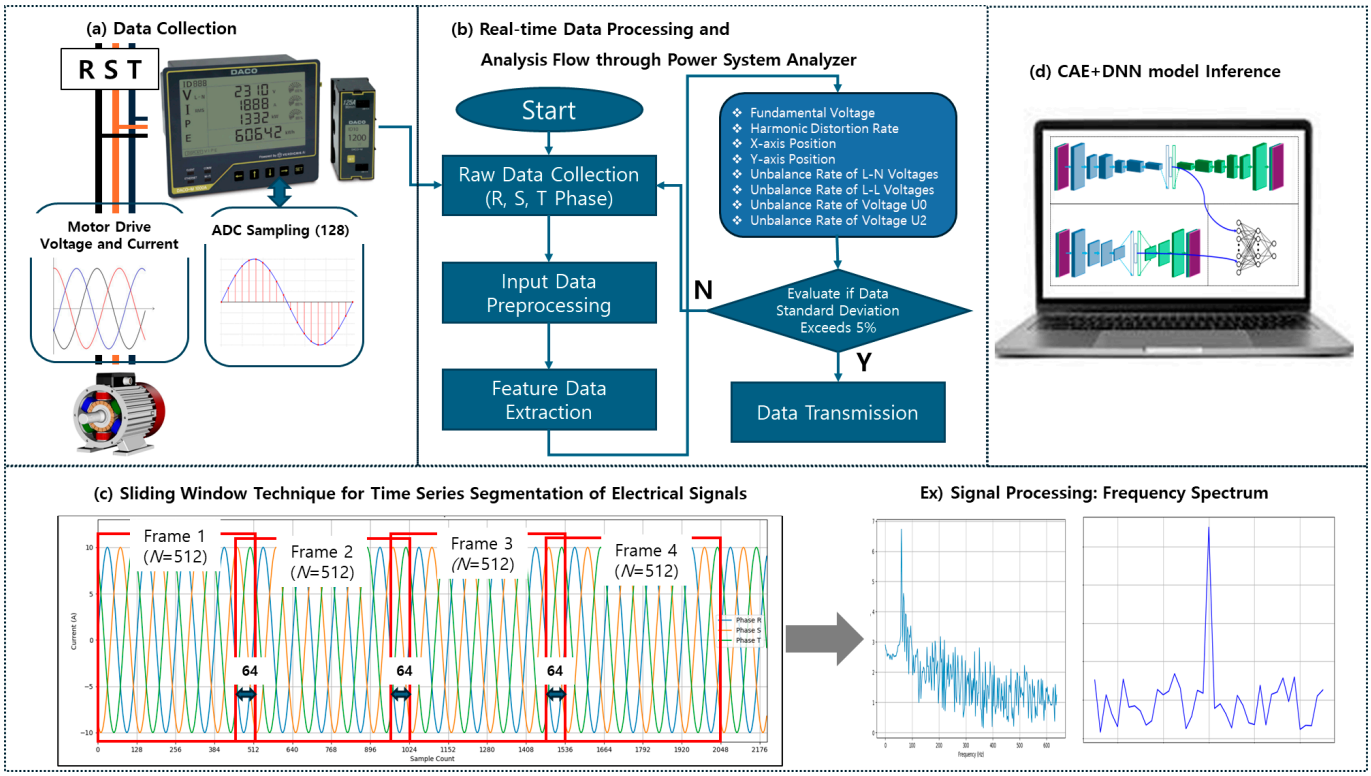

Figure 1. Data processing and analysis flow for electric motor fault diagnosis; (**a**) data collection, (**b**) real-time data processing and analysis flow through power system analyzer, (**c**) sliding window technique for time-series segmentation of electrical signals, and (**d**) CAE + DNN model inference.

In summary, the contributions of this study are as follows:

1. Data Feature Extraction and Real-time Processing: Extract power system analysis data from raw electrical energy signals, minimizing the delay in fault diagnosis through real-time data processing.

2. Development of a High-Precision Deep Learning Model: Develop a high-precision model for the early diagnosis of electric motor faults using a CNN autoencoder. This model effectively learns and analyzes complex patterns in electrical energy data, surpassing methods that rely on empirical knowledge or threshold values.
3. Industrial Application: Apply the proposed method to motors and mechanical systems to evaluate its practicality and effectiveness in real industrial environments.

This paper is structured as follows: Section 2 reviews related research, Section 3 explains the proposed research methodology and procedures, Section 4 presents experiments and results, and finally, Section 5 discusses the conclusions and future research directions.

2. Literature Review

This section analyzes how advancements in artificial intelligence (AI), particularly machine learning technologies, have transformed fault diagnosis in industrial systems. The study reviews the latest machine learning methodologies introduced to overcome the limitations of traditional fault diagnosis methods and discusses the major benefits and potential limitations that have arisen during this technological transition.

2.1. Importance and Technological Advances in Fault Diagnosis

Fault diagnosis has evolved from initial manual inspection methods to the adoption of advanced diagnostic technologies. These technologies provide highly reliable results, thereby reducing fault prediction times and minimizing downtime, which in turn decreases productivity losses [10]. Additionally, the application of various signal processing techniques and artificial intelligence has introduced cutting-edge technologies that effectively handle complex data and enable precise fault detection. These technological advancements enhance the efficiency and accuracy of motor fault diagnosis, contributing to increased reliability in industrial environments [11].

2.2. Traditional Diagnostic Methods and Signal Processing-Based Approaches

Traditional motor fault diagnosis primarily relied on physical inspections and preventive maintenance, which often led to unnecessary replacements and high costs [6]. Motor Current Signal Analysis (MCSA) is a reliable non-invasive method that detects mechanical and electrical faults by analyzing current signals. While it is cost-effective, its limitations include low sensitivity to early-stage faults and the inability to collect high-resolution data in the frequency domain. Additionally, it may face constraints when applied to electrical loads outside of the motor [7].

Signal processing-based methods analyze faults in the time, frequency, and time–frequency domains. Time domain analysis uses RMS and peak values, frequency domain analysis employs FFT, and time–frequency analysis utilizes STFT and CWT [12]. Although these methods are cost-effective, they have limitations in processing complex patterns in real time [13,14]. To address these challenges, machine learning-based approaches have been developed.

2.3. Data-Centric Approach

Recently, data-driven approaches have emerged as effective alternatives to overcome these limitations [15,16]. With advancements in sensor technology and data processing capabilities, the real-time analysis of multivariate data has become feasible, enabling more precise early detection and prediction of fault patterns [17,18]. Data-driven technologies leverage machine learning algorithms to learn patterns from fault data, significantly improving the accuracy and efficiency of predictive maintenance [19–21].

2.4. Importance of Data Preprocessing and Transformation

Data preprocessing is essential for enhancing the accuracy of fault pattern recognition and fault diagnosis. Raw data can contain noise and missing values, necessitating a process to transform it into an analyzable form [22–24]. Effective data preprocessing significantly

improves the accuracy of fault diagnosis and increases the reliability of the system [25]. The impact of normalization, scaling, and noise removal on fault pattern recognition has been analyzed [26,27]. Modulated time–frequency feature analysis is useful for precisely diagnosing faults in complex systems [28–30]. Advanced preprocessing techniques, such as multi-scale analysis, extract features at various scales, thereby increasing the sensitivity of fault diagnosis [31,32].

2.5. Integrated Analytical Methodology Utilizing Machine Learning

For fault diagnosis in complex systems, integrated approaches based on machine learning are becoming increasingly important [33]. By combining modulated time–frequency features with deep residual learning, gearbox faults have been precisely diagnosed, enhancing diagnostic accuracy by comprehensively considering the temporal and frequency variations of signals [34]. Additionally, dynamically weighted wavelet coefficients and deep residual networks have been used to effectively detect faults under various operating conditions [35]. Intelligent monitoring and diagnostic systems based on deep learning have been developed to fuse features from multiple sensor data, enabling more accurate fault diagnosis in complex systems [36,37].

2.6. Classifier Construction

The construction of classifiers is a crucial step in fault diagnosis systems, enabling the accurate determination of faults based on identified features. Recent studies have employed various neural network architectures for this purpose, each demonstrating different characteristics and performance.

- Convolutional Neural Networks (CNNs): While CNNs are primarily strong in processing image data, they also exhibit effective feature extraction capabilities for time-series data. This is particularly useful in fault diagnosis, allowing for the effective learning of both visual and temporal patterns in data [38,39].
- Recurrent Neural Networks (RNNs) and Long Short-Term Memory (LSTM) Networks: RNNs and LSTMs excel in capturing the temporal continuity and context of time-series data. This makes them suitable for monitoring dynamic changes in mechanical systems like electric motors, allowing for the early detection of fault symptoms by capturing long-term dependencies [40].
- Autoencoders for Anomaly Detection: Autoencoders are used to detect anomalies by compressing and reconstructing the key features of input data. In fault diagnosis, autoencoders identify abnormal patterns and predict faults by highlighting deviations from normal operational states [41,42].

2.7. Signal Analysis Methods for Motor Drives

The provided Figure 2 shows that the signal analysis of motor drives is mainly divided into the time domain, frequency domain, and time–frequency domain analyses. In time domain analysis, indicators such as peak, RMS, and crest factor are used to identify mechanical faults. Frequency domain analysis employs FFT and cepstrum analysis to precisely detect anomalies at specific frequencies [43]. Time–frequency analysis captures the dynamic changes in the system and identifies complex fault patterns using STFT, CWT, and HHT [44,45]. These multifaceted analysis methods are essential for fault diagnosis in motor drives, and an integrated approach maximizes diagnostic precision [46,47].

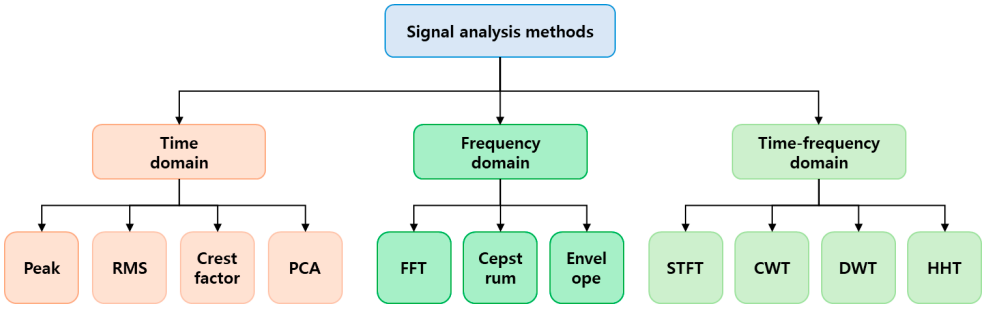

Figure 2. Signal analysis methods for motor drives.

2.8. Data-Driven Motor Fault Diagnosis

Table 1 summarizes the approaches, sensors used, experimental data, and the innovation and practical applicability of the results from recent studies.

Table 1. Comparison of recent studies on electric motor fault diagnosis.

Publication Year, Number of References,	Fault Type	Analysis Data Type	Innovation and Approach	Performance and Application Cases
2021, 32 [48]	Early, Mid, and Permanent Faults	Raw data collected from vibration sensors and acoustic emission sensors	Based on Bayesian Network Data-driven Initial Fault Diagnosis Wavelet Threshold Noise Reduction Minimum Entropy Restoration	Initial Fault Diagnosis Accuracy over 90%, (1)
2021, 23 [49]	Rotating Machinery Faults	Vibration signal data collected from a vibration sensor installed on the motor drive end bearing	PdM-CNN Model Predictive Maintenance Model Tested Under Various Rotational Speeds, Loads, and Severity Conditions	Achieved 99.58% Accuracy and 97.3%, (1)
2023, 41 [50]	Bearing Faults	Raw vibration signal data collected from a bearing vibration sensor	Time–Frequency Information Fusion Wavelet Packet Decomposition and Reconstruction Improved Maximum Mean Discrepancy Algorithm Applied	High Diagnostic Accuracy and Strong Robustness, (1)
2022, 48 [51]	Bearing Faults	Raw vibration signal data collected from a bearing vibration sensor	Multitask Attention CNN (MTA-CNN) Utilized GFS-Network and FLA-Module Information Sharing Across Multiple Tasks	Superior Performance Compared to State-of-the-Art Deep Learning Methods, (1)
2023, 30 [52]	Bearing Faults	Raw vibration signal data collected from a bearing vibration sensor	Feature Extraction through CWT and Image Transformation Using Gaussian CDBN Low Signal–Noise Ratio Conditions	Excellent Performance under Various Operating Conditions, (1)
2021, 206 [53]	Mechanical and Electrical Faults	Hybrid signal processing data including both vibration and current signals	Vibration-based Methods Current Signal-based Methods Use of Hybrid Signal Processing and AI Techniques	Excellent Diagnostic Performance under Various Conditions, (1) Potential for Application in Electric Vehicles
2021, 29 [54]	Initial Winding Faults	Raw flux signal-based data collected from three positions of the machine	Flux Monitoring Methods Real-time Fault Detection without External Resistors High-Reliability Verification in Various Low-Level Faults	Detection of low-Level Winding Faults There is Potential for Practical Application
2020, 18 [55]	Bearing Faults	Raw vibration signal data collected under varying speed conditions	Spectrogram Generation using STFT Using CNN and VGG16 High Accuracy under Various Rotational Speeds	High Accuracy and Robustness, (1)

Table 1. *Cont.*

Publication Year, Number of References,	Fault Type	Analysis Data Type	Innovation and Approach	Performance and Application Cases
2020, 25 [56]	Bearing Faults	Raw vibration signal data collected from an accelerometer	Feature Extraction using Autocorrelation Using Random Forest Classifier Fault Diagnosis under Various Conditions	High Diagnostic Accuracy, (1)
2020, 61 [57]	Initial Winding Faults	Raw current signal data (direct processing)	CNN-based Fault Detection and Classification Direct Processing of Raw Current Data Tested under Various Load Torque and Supply Voltage Frequency Conditions	High Detection Accuracy for Initial Winding Faults, (1)

(1) No Practical Applications Noted.

Traditional motor fault diagnosis methods are primarily based on empirical knowledge or threshold values. These approaches have limitations in effectively identifying and predicting various fault types that occur in complex motor systems [10]. To overcome these limitations, recent studies have applied advanced technologies. For example, Zhao et al. developed a method that extracts features from vibration amplitude spectrum images using continuous wavelet transform and a Gaussian Convolutional Deep Belief Network (CDBN). This method enables effective bearing fault classification even under low signal–noise ratio conditions, overcoming the limitations of traditional manual feature extraction [52]. Additionally, Wang et al. developed a Feature-Level Attention-Guided Multitask Convolutional Neural Network (MTA-CNN), which demonstrated superior performance in fault diagnosis and operating condition identification for bearings compared to the existing deep learning methods. This model improved fault diagnosis accuracy under various conditions by using a Global Feature Sharing network (GFS-network) and task-specific networks [51].

Additionally, the PCCDP method analyzed three-phase current signals and proposed a predictive maintenance system aimed at reducing equipment downtime [58]. The image processing technique combining InceptionV3 and CLA-HE, coupled with SVM, further enhanced diagnostic performance [59]. While RNN and LSTM models excel in handling time-series data, CNN is more suited for motor fault diagnosis in terms of frequency component analysis and spatial pattern recognition [58]. CNN effectively extracts complex patterns [59], and the autoencoder improves diagnostic accuracy by denoising and compressing features during this process [60]. DNN further enhances the precision of fault diagnosis by learning these high-dimensional features [61].

However, these technologies still exhibit limitations in processing speed and data complexity, and the accurate classification and prediction of fault types remain challenges to be addressed. This study aims to overcome these limitations by proposing a structure that combines autoencoders and DNNs to maximize performance. It is expected that developing optimized power system data acquisition equipment will improve data processing efficiency and further enhance the accuracy of fault diagnosis.

3. Research Methodology

This study explains the process of electric motor fault diagnosis step by step, covering the stages from data collection to real-time processing and analysis, and finally to fault diagnosis. The key stages consist of data collection, real-time data processing through a power system analyzer, and fault diagnosis using a CNN-based autoencoder and DNN model.

Figure 3 visually explains each stage, illustrating the entire process from data collection to final fault diagnosis.

- (a) Data Collection: Accurately measures voltage and current data from the electric motor, providing fundamental data for motor condition monitoring.
- (b) Real-Time Data Processing and Analysis: Processes data in real-time using a power system analyzer, monitoring and analyzing the electrical system's condition.
- (c) Signal Processing Structure: Structures the R, S, and T phases like RGB channels to prepare the data for CNN to learn patterns.
- (d) Time-Series Data Segmentation Using Sliding Window Technique: Segments the data in time-series to analyze complex patterns more precisely and efficiently.
- (e) CAE (CNN Autoencoder) Structure: Processes raw data and power system data using the CNN autoencoder, extracting critical features to identify patterns that enable early fault detection.
- (f) DNN-Based Fault Diagnosis: Combines the key features extracted by the CAE with the DNN to diagnose faults, improving diagnostic accuracy.

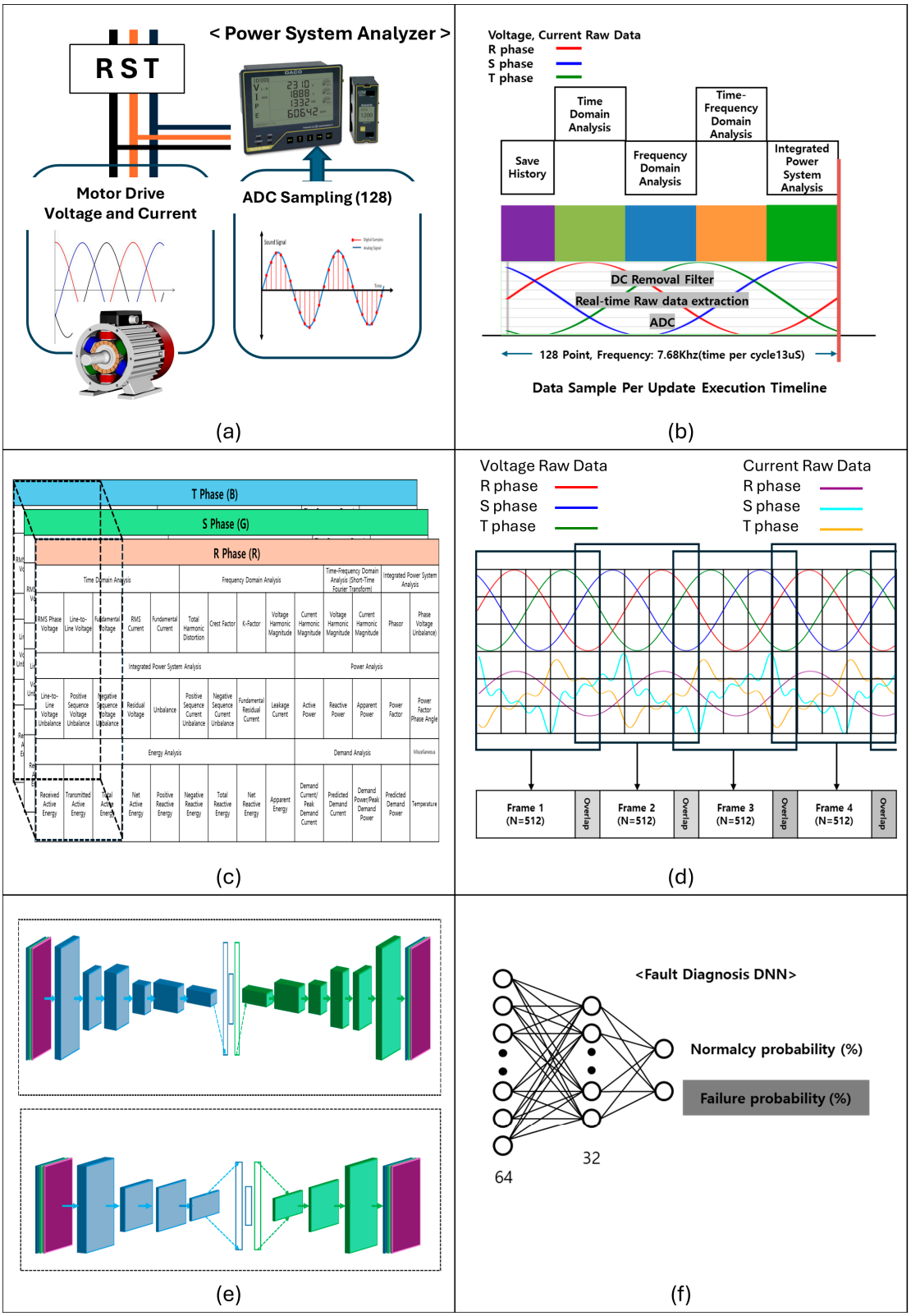

Figure 3. Visualization of the electric motor fault diagnosis process using CNN autoencoder and DNN: (**a**) data collection; (**b**) real-time data processing and analysis flow through power system analyzer; (**c**) CNN data structure of power system analysis data; (**d**) sliding window technique for time-series segmentation of electrical signals; (**e**) CAE structure for raw data and power system analysis data; (**f**) DNN structure combining CAE features.

3.1. Experimental Setup and Data Processing

In this study, voltage and current data were collected using the CTSR 0.3-P current transformer (CT) from LEM. This sensor offers a high accuracy of ±0.1% and a wide operating range, capable of measuring currents from 0.1 A to 30 A. The CTSR 0.3-P sensor provides stable performance at frequencies of 50 Hz and 60 Hz, and accurate data across a wide temperature range (−40 °C to 85 °C). These characteristics make this sensor highly suitable for monitoring the performance of electric motors in various environments.

As shown in Figure 4, the experimental setup is connected to various power analysis devices to collect and analyze data for motor fault diagnosis. Analog signals are digitized at 7.68 kHz using the ADS1256 high-precision analog-to-digital converter (A/D), which offers 24-bit resolution and low-noise characteristics, enabling precise data collection. According to Nyquist's theorem, the sampling frequency is set to twice the maximum frequency of the signal to ensure accurate signal reconstruction.

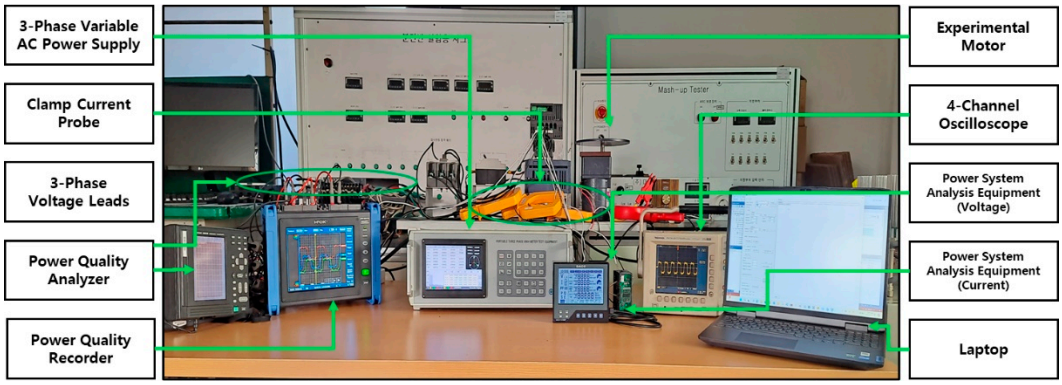

Figure 4. Experimental equipment configuration diagram.

Figure 5 illustrates the process of digitizing the raw voltage and current data from the R, S, and T phases generated by the motor using a high-precision analog-to-digital converter (ADC). These data are then passed to the power system analysis process for the analysis of FFT, THD, and phase unbalance. After the analyzed data are validated for accuracy using standard deviation information, it is transmitted to a PC via Ethernet for real-time monitoring and analysis.

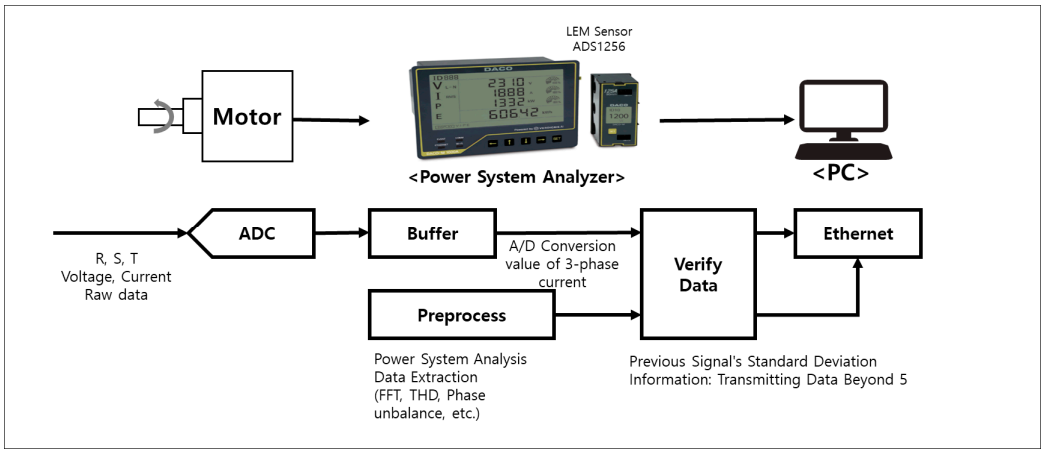

Figure 5. Data collection process.

The power system analyzer continuously monitors key metrics such as voltage unbalance ratio and harmonic distortion ratio. If the standard deviation of the voltage or current data exceeds 5%, it is recognized as an abnormal signal, and data from the previous 10 cycles, including the abnormality, is transmitted to the model inference stage. At

this point, the sliding window algorithm is employed to continuously analyze the data, enabling the rapid detection of abnormal states. Additionally, a Z-score-based algorithm evaluates the normal range of the data in real time, and if the Z-score exceeds ±3, the data are immediately classified as abnormal. These two algorithms work complementarily to quickly detect and handle abnormal data.

3.2. Introduction to the Dataset

In this study, raw voltage and current data were collected from the 'TG-55L' motor manufactured by Tsukasa Electric. Using a power system analyzer and LEM's CTSR 0.3-P current transformer, we secured stable data within the range of 0.1 A to 30 A, with a high accuracy of ±0.1%. The primary fault types are bearing failure (69%), misalignment (21%), and shaft imbalance (7%), with bearing failure being the most prevalent. It is known to cause abnormal patterns and increased harmonic components in the current signal [62]. Additionally, misalignment and shaft imbalance lead to electromagnetic force imbalance, affecting the voltage and current signals, thereby reducing motor stability [63]. Consequently, this study focuses on analyzing these three fault types.

The experiment was conducted using the TG-55L motor model. Table 2 shows the technical specifications of the TG-55L motor used in this study. Based on the characteristics of the collected power system analysis data, the proposed model is expected to generalize across various motor types. Future studies are needed to verify the model's generalizability with different motors, and such validation is expected to enable the application of the study's findings in various industrial settings.

Table 2. Motor technical specifications.

Rated Voltage	No-Load Speed (r/min)	No-Load Current (mA)	Torque		Rated Speed	Rated Current (mA)
			(mN · m)	(gf · cm)		
24	3900	85	19.6	200	2650	420

Each fault type was physically reproduced, and data were collected using a power system analyzer. Bearing failure was measured by detecting abnormal rotation due to bearing wear, while misalignment was recorded through changes in electrical characteristics from shaft-rotor imbalance. Shaft imbalance data were captured by observing irregular voltage and current fluctuations caused by asymmetric shaft loading.

The data were collected under the following conditions:

- Sensors: Voltage and current data were collected using LEM's CTSR 0.3-P current sensor, and each fault type was tested separately.
- Load conditions: The motor was tested under both no-load and full-load conditions.
- Sampling rate: The experimental data were sampled at 7.68 kHz, and each experiment was conducted over a period of 10 h.
- Data size: The data collected for each fault condition consisted of approximately 51,000 cycles of samples.
- Data segmentation: The collected raw data were segmented into 512-point units and processed using a sliding window technique with overlapping to enhance the reliability of fault diagnosis.

3.3. Real-Time Data Processing

Figure 6 visually illustrates the process of real-time data processing and analysis using the proposed CNN autoencoder model in the power system. The system collects voltage and current data from the R, S, and T phases at a speed of 7.68 kHz per second and processes the data during one cycle (13.6 μs) at 60 Hz to diagnose motor faults.

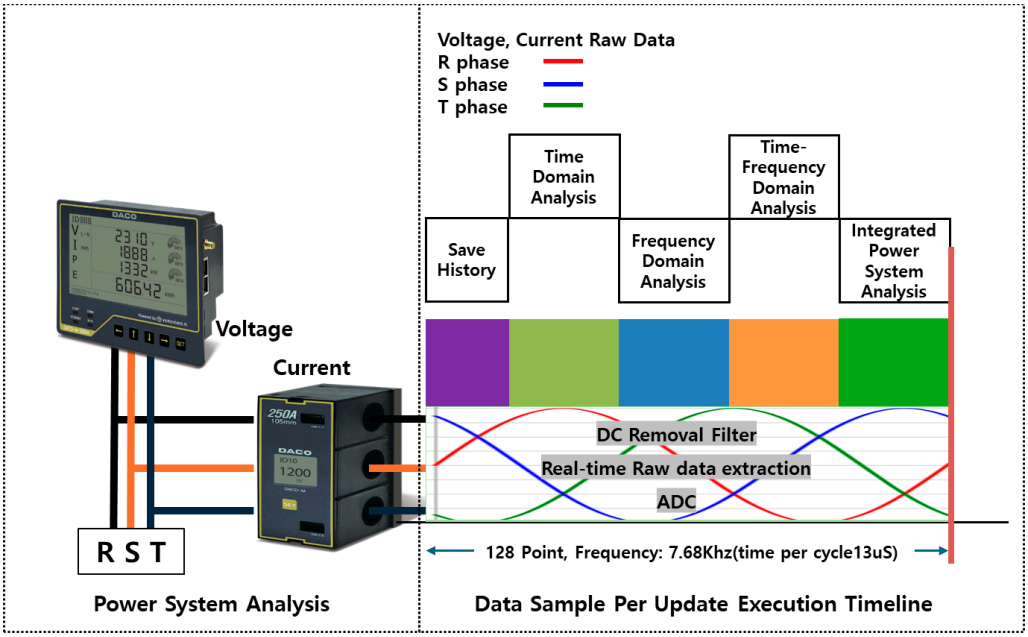

Figure 6. Real-time data processing and analysis using the power system analyzer.

- Real-time Raw Data Extraction: Voltage and current data from the R, S, and T phases are digitized at a speed of 7.68 kHz per second, providing the foundational data for real-time analysis.
- DC Removal Filter: The DC component is removed from the raw data to reduce noise, and the filtered data are used for time and frequency domain analysis.
- Time Domain Analysis: Based on the DC-filtered data, the system analyzes RMS values, phase voltage, and current variations to detect abnormal motor conditions.
- Frequency Domain Analysis: The system extracts frequency components using FFT, calculating metrics such as total harmonic distortion (THD) and crest factor.
- Time–Frequency Domain Analysis: STFT and wavelet transformations are employed to combine time and frequency information for precise signal analysis.

As part of this study, a digital power analyzer was developed to extract and analyze data from the entire power system. The digital power analyzer processes real-time data at 7.68 kHz and contributes to power quality monitoring, load management, and system optimization. The combined CNN autoencoder and DNN model significantly improves accuracy and speed over traditional diagnostic methods. This approach aids in reducing maintenance costs, optimizing energy consumption, and supporting strategic decision-making.

3.4. Power System Analysis Data

The power system analysis data extracted from the raw data are precisely analyzed by the second CNN. This process evaluates phase voltage, line-to-line voltage, fundamental wave voltage, total harmonic distortion (THD), phasor, voltage imbalance, RMS current, harmonic current, and current imbalance. For example, phase voltage imbalance (NEMA MG1) is defined as the ratio of the maximum deviation to the average line voltage, indicating inefficient motor operation and risk of failure. The THD of the current, representing the ratio of harmonic current to the fundamental wave, is a crucial indicator of power quality degradation and potential motor damage. Table 3 describes the power system analysis data signal analysis techniques applied in this study for fault diagnosis.

Table 3. Signal analysis items for motor fault diagnosis using power system analysis data.

Category	Item	Description
Time Domain Analysis	RMS Phase Voltage	The effective voltage of each phase
	Line-to-Line Voltage	Voltage between two phases
	Fundamental Voltage	Voltage of the main frequency component
	RMS Current	Effective current of each phase
	Fundamental Current	Current of the main frequency component
Frequency Domain Analysis	Total Harmonic Distortion (THD)	Total harmonic distortion ratio
	Crest Factor	Ratio of peak voltage to RMS voltage
	K-Factor	Evaluation of harmonic current load on the transformer
Time–Frequency Domain Analysis	Voltage Harmonic Magnitude	Harmonic voltage magnitude up to the 31st order
	Current Harmonic Magnitude	Harmonic current magnitude up to the 31st order
Integrated Power System Analysis	Phasor, Vector Diagram	Magnitude and phase of voltage and current
	Phase Voltage Unbalance	Phase voltage unbalance according to NEMA MG1 standards
	Line-to-Line Voltage Unbalance	Line-to-line voltage unbalance according to NEMA MG1 standards
	Positive Sequence Voltage Unbalance	Positive sequence voltage unbalance
	Negative Sequence Voltage Unbalance	Negative sequence voltage unbalance
	Residual Voltage	Residual voltage of the system
	Current Unbalance	Current unbalance according to NEMA MG1 standards
	Positive Sequence Current Unbalance	Positive sequence current unbalance
	Negative Sequence Current Unbalance	Negative sequence current unbalance
	Fundamental Residual Current	Residual current of the fundamental frequency component
Power Analysis	Active Power	Actual power consumed
	Reactive Power	Power that does not perform actual work but is necessary for system stability
	Apparent Power	Sum of active power and reactive power
	Power Factor	Power efficiency index
	Power Factor Phase Angle	Phase angle between voltage and current
Energy Analysis	Received Active Energy	Received active energy
	Transmitted Active Energy	Transmitted active energy
	Total Active Energy	Total active energy
	Net Active Energy	Net active energy
	Positive Reactive Energy	Positive reactive energy
	Negative Reactive Energy	Negative reactive energy
	Total Reactive Energy	Total reactive energy
	Net Reactive Energy	Net reactive energy
	Apparent Energy	Apparent energy
Demand Analysis	Demand Current/Peak Demand Current	Predicted current and peak current
	Predicted Demand Current	Predicted current
	Demand Power/Peak Demand Power	Predicted power and peak power
	Predicted Demand Power	Predicted power
Other	Surface Temperature	Measurement of surface temperature

- *RMS* (Root Mean Square): This is a measurement method used to represent the average magnitude of voltage or current. It is the square root of the mean value of the squares of a periodic waveform. RMS reflects the average magnitude of periodic voltage and current signals, enabling the assessment of the motor's condition.

$$X_{RMS} = \sqrt{\frac{1}{T}\int_0^T X(t)^2 dt}, \qquad \text{where } x = V(t), \mathrm{I(t)} \tag{1}$$

- Fundamental and Harmonic Analysis: Analyzing the frequency components of the fundamental and harmonic waves to evaluate whether the motor is operating normally or if there are any faults. Harmonic analysis is particularly useful for detecting the early signs of faults.

$$X(t) = X_0 + \sum_{n=1}^{50} [X_n \cos(n\omega_0 t + \varnothing_n)], \quad \text{where } x = V(t), \mathrm{I(t)} \tag{2}$$

- Phasor: A complex vector used to simply represent waveforms that change over time. A phasor summarizes the amplitude, phase, and frequency of a waveform, making it useful for simplifying the analysis and design of circuits in electrical engineering.

$$A\angle\theta = A(\cos(\theta) + j\sin(\theta)) = Ae^{j\theta} \tag{3}$$

- Total Harmonic Distortion (THD): An indicator that expresses the effect of frequency components other than the fundamental frequency on the overall signal as a percentage. In power systems, THD is crucial for evaluating power quality and can cause performance degradation or damage to electrical equipment. THD is calculated by taking the sum of the power of all the harmonic components relative to the fundamental power, and expressing this ratio as a percentage.

$$THD = \frac{\sqrt{\sum_{k=2}^{31} X_k^2}}{X_1}, \quad \text{where } x = V, \mathrm{I} \tag{4}$$

- Total Demand Distortion (TDD): Represents the ratio of harmonic current to the total load current, calculated with respect to the maximum demand current. This indicator evaluates the overall harmonic distortion burden on the power system and is essential for ensuring compliance with power quality standards. According to the IEEE 519 standard, TDD is a key criterion for assessing whether the design and operational standards related to harmonic management are met.

$$TDD = \frac{\sqrt{\sum_{k=2}^{31} I_k^2}}{I_L} \tag{5}$$

- Unbalance of Voltage and Current: Occurs when phases in an electrical system are not separated by the ideal 120-degree phase angle. This can reduce the efficiency of machines like motors, and cause overheating and faults. Voltage unbalance is defined by the NEMA MG1 standard and is measured as the ratio of the maximum deviation to the average line voltage.

$$I_1 = \frac{I_a + I_b + I_c}{3} \tag{6}$$

$$I_2 = \frac{I_a + a^2 I_b + a I_c}{3}, \text{ where } a = e^{j\frac{2\pi}{3}} \tag{7}$$

- Active Power: Measures the active power actually consumed by the motor to evaluate energy efficiency.

$$P_x = \frac{1}{T}\int_0^T V_x(t) I_x(t) dt, \text{ where } x = R, S, T \tag{8}$$

- Reactive Power: Measures reactive power to assess power quality and energy loss.

$$Q_x = \frac{1}{T}\int_0^T V_x\left(t - \frac{T}{4}\right) I_x(t) dt, \text{ where } x = R, S, T \tag{9}$$

- Apparent Power: Measures apparent power to evaluate the total power consumption of the motor and to understand the overall condition of the power system.

$$V_{x,rms} = \sqrt{\frac{1}{T}\int_0^T v_x^2(t)dt}, \quad I_{x,rms} = \sqrt{\frac{1}{T}\int_0^T i_x^2(t)dt}, \quad \text{where } x = R, S, T \tag{10}$$

- Power Factor: Measures the power factor to evaluate the efficiency of power usage and to comprehensively analyze the power quality of the system.

$$PF_x = \frac{P_x}{S_x}, \qquad \text{where } x = R, S, T \tag{11}$$

3.5. Power System Analysis Data Structure

This section introduces data specialized for electrical parameters. It is designed considering the unique characteristics of electrical parameters that differentiate it from conventional raw data-based models.

As shown in Figure 7, each R, S, and T phase of the electrical system is treated like the RGB channels in image processing, effectively analyzing the interactions between data. The power system analysis data are arranged so that related items for each phase are adjacent, providing an ideal structure for the CNN to learn complex patterns, similar to object detection or edge detection in image processing. Furthermore, various signal processing techniques such as time domain, frequency domain, and time–frequency domain analysis (STFT) are applied to analyze electrical energy data.

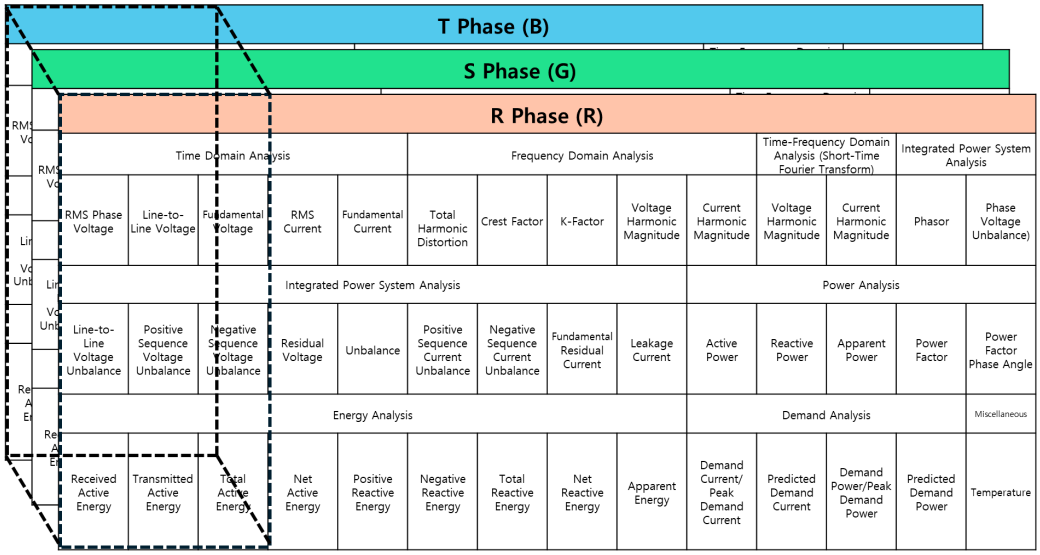

Figure 7. Signal processing architecture of power system analysis data.

This method allows for the precise detection of faults in the electrical system and clearly analyzes the impact of electrical parameters on fault diagnosis. It is expected to improve accuracy and reliability in practical applications. The in-depth analysis of power data provides the technical basis and methodology necessary for efficient electrical system management and fault detection. This integrated approach can be utilized in various applications, including fault diagnosis and predictive maintenance. This analysis helps evaluate the quality and efficiency of the power system, understand various elements, and contribute to motor fault diagnosis and analysis of different load conditions.

3.6. Sliding Window Technique

Figure 8 shows an example of time-series data segmentation using the sliding window technique. This method allows the flexible segmentation of data while preserving the

temporal structure of the time-series, making it applicable to various analysis scenarios. In this study, the window size was set to 512 sampling points. This size was chosen to enable the CNN autoencoder model to effectively capture the important frequency components and patterns in motor fault diagnosis.

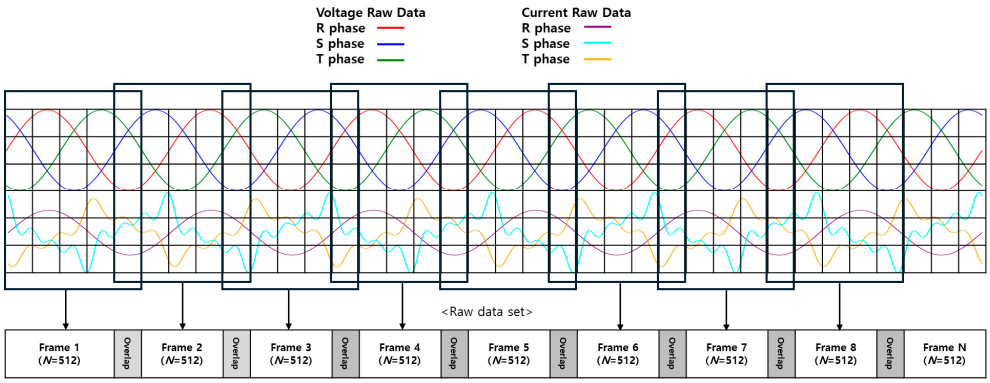

Figure 8. Sliding window technique for time-series segmentation of electrical signals.

The selected window size offers an optimal balance between computational efficiency and performance, and it is advantageous for detecting frequency variations and pattern recognition across various signals [64]. The data are transformed from one-dimensional to two-dimensional form, and each window is used for anomaly detection and data replacement while maintaining the continuity of the data stream. The window size and overlap are represented by the following equation [65].

$$x_i = [x_{iS} + 1(k), x_{iS}2(k), \ldots, x_{iS} + W(k)] \tag{12}$$

Here, i represents the window index, S is the step size (the interval for moving to the next window), W denotes the window size, and k represents the data stream. This configuration maintains the temporal continuity of the data while adjusting the window size and overlap to flexibly respond to various data patterns. This method effectively extracts important information from the raw voltage and current data, balancing analysis accuracy and processing efficiency by handling subtle changes and noise. Figure 9 provides an example of how the method is applied in this study.

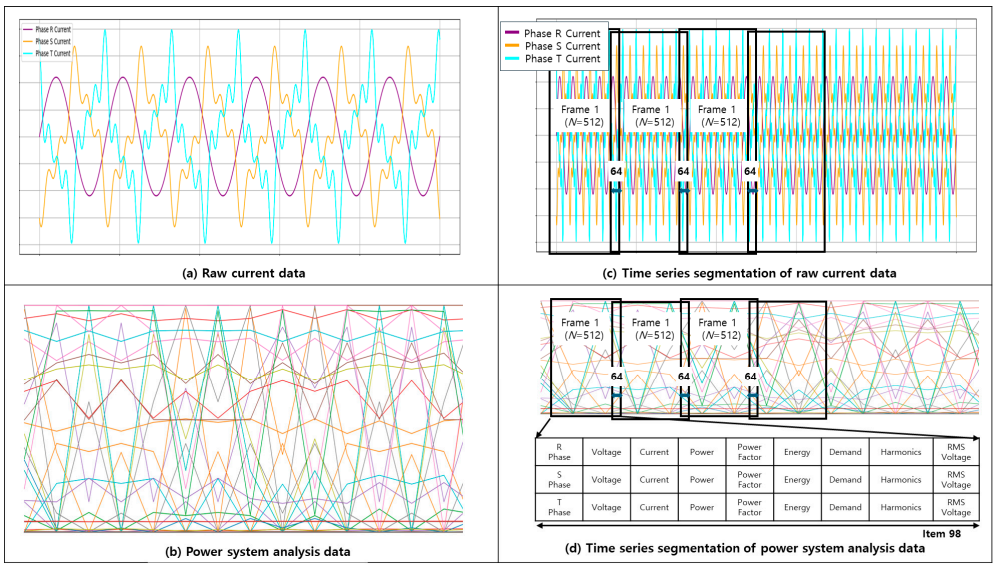

Figure 9. Sliding window of entire data: raw data and power system analysis data. (**a**) The raw current data visually represents the raw data of the R, S, and T three-phase currents, which are the

real-time measurements of the motor's condition and form the basis for fault analysis. (**b**) The power system analysis data includes various power quality and analysis data extracted from the power system, such as current and voltage imbalance and harmonic analysis, which are used in conjunction with the current data to detect abnormal signs. (**c**) The raw current data are segmented into fixed frames using the sliding window technique, allowing for the precise analysis of anomalies. The frame size is set to 512 samples, with each frame processed with an overlap of 64 samples. (**d**) The power system analysis data are also synchronized with the raw current data and processed using the sliding window technique.

3.7. Model Structure and Proposed Method

In this study, a combination of a CNN autoencoder and a DNN is used to diagnose faults in electric motors. The CNN autoencoder effectively extracts critical information from the raw data and power system analysis data, transforming it into a lower-dimensional latent space. These extracted features are then passed to the DNN, which models complex nonlinear relationships and enables precise fault diagnosis.

As shown in Figure 10, the proposed model consists of two CNN autoencoders and a DNN. The first CNN autoencoder processes the sinusoidal raw data of the R, S, and T phase currents, while the second CNN autoencoder processes the power system analysis data. These two autoencoders extract key features and transform them from high-dimensional to low-dimensional latent spaces. The latent features are then passed through fully connected layers to the DNN. The DNN integrates the raw data and power system analysis data to quickly distinguish between normal conditions and potential faults.

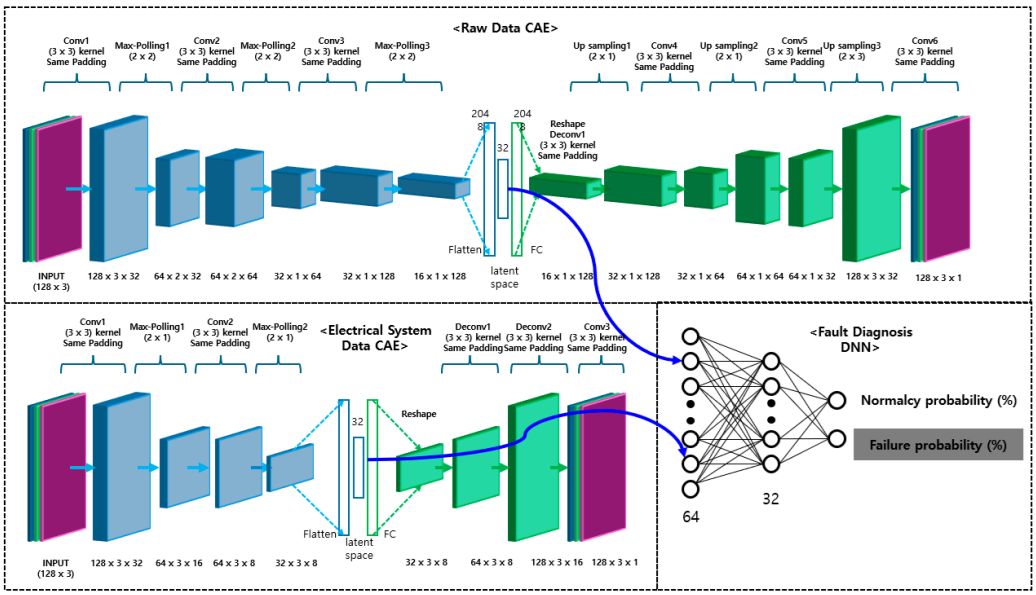

Figure 10. Combined CAE and DNN structure for electrical signal analysis.

3.7.1. CNN Autoencoder

The CNN autoencoder model collects sinusoidal current signals and power system data to extract the motor's fundamental power data and analyze patterns from this information. Figure 11 illustrates the CAE structure used for processing such raw data.

Figure 12 depicts the CAE structure used for processing power system analysis data. After undergoing initial preprocessing, the multidimensional input data $X \in \mathbb{R}^{w*h*c}$ is fed into the encoder. Here, w, h, and c represent the width, height, and number of channels of the data, respectively. These data are transformed into a lower-dimensional feature space

through multiple layers of the encoder, reducing its dimensionality while preserving the important information from the original data [65].

$$X \in \mathbb{R}^{w*h*c} \tag{13}$$

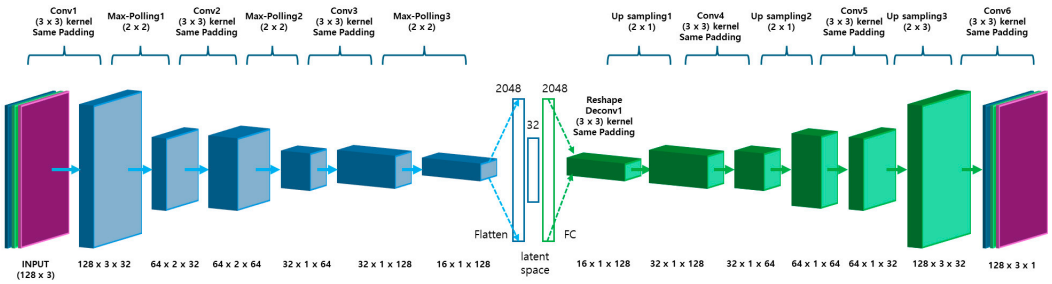

Figure 11. CAE structure of raw data.

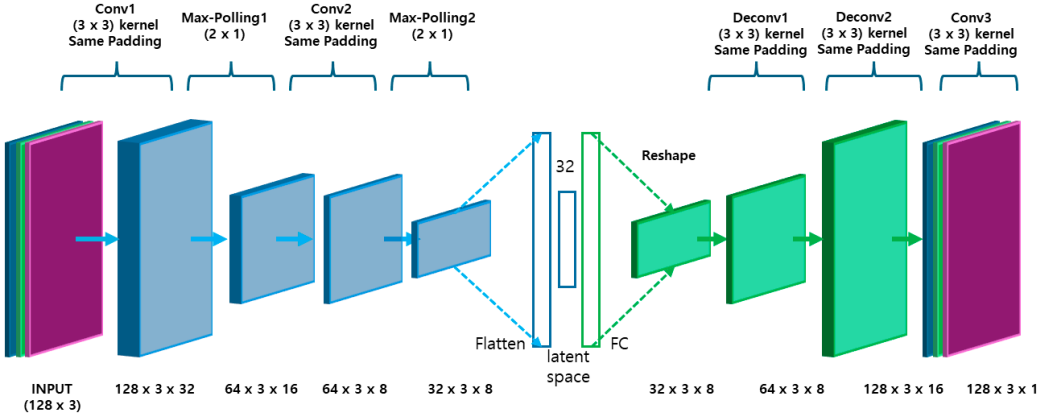

Figure 12. CAE structure of power system analysis data.

Convolution Operation: The input data passes through multiple convolutional layers, where each layer uses K convolutional filters of size F × F × c to extract important features from the spatial structure of the data. This process generates feature maps that enhance the level of abstraction of the data.

Data Segment Partitioning: The data are partitioned using a slicing technique, defined based on a specific 'window size' W and 'overlap' O. The actual slice interval is set to $W - O$, and data segments are generated using the following formula:

$$step\_size = W - O \tag{14}$$

Here, $step\_size = W - O$ represents the interval between slices. This method helps maintain data continuity while effectively extracting necessary parts for analysis preparation.

Data Slicing: When the length of the dataframe is N, slicing is performed using the following formula:

$$segments = \{data[i : i + W] | i \in [0, N - W + 1, step\_size]\} \tag{15}$$

Through multiple convolutional layers, the data are filtered, with each layer applying the nonlinear activation function ReLU to enhance the features. The convolution operation transforms the data into characteristic elements, and then reduces the spatial dimensions through pooling operations. These transformed data are passed to the next layer, focusing on simplifying complex input data while preserving key features.

$$X^{(l+1)} = ReLu\Big(Conv\Big(X^{(l)}\Big)\Big) \tag{16}$$

The decoder reconstructs the high-dimensional features back into the original data, restoring details through transposed convolution (ConvTranspose) and ReLU activation functions. During the optimization process using the Adam optimizer, early stopping and dropout techniques were applied to prevent overfitting and optimize model performance.

$$X^{(l-1)} = ReLu\left(ConvTranspose(X^{(l)})\right) \tag{17}$$

Here, 'ConvTranspose' refers to the transposed convolution operation, and $X(l)$ is the output of the l-th layer.

3.7.2. Feature Combination of Autoencoders through DNN

As shown in Figure 13, thefeature vectors extracted fromthe two CNN autoencoders are combined using a deep neural network (DNN) integrated with a multilayer perceptron (MLP) architecture to maximize fault diagnosis accuracy. The DNN learns the complex interactions of the data using two dense layers and the ReLU activation function, and finally predicts the motor's status through a softmax output layer. This process is designed to minimize the loss of multi-class classification using sparse categorical cross-entropy and optimize the model with the Adam optimizer.

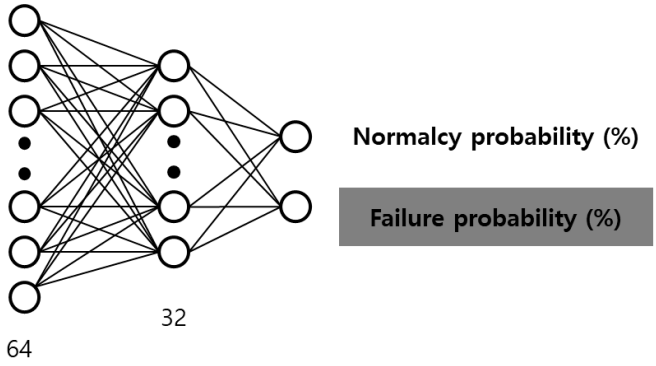

Figure 13. DNN structure combined with CAE features.

The two CAEs were kept fixed, and Bayesian Optimization was applied to optimize the performance of the DNN model. Bayesian Optimization is an efficient method for exploring the hyperparameter space by focusing on promising regions. In this study, the optimized hyperparameters were the learning rate, the number of neurons in the hidden layers, and the dropout rate. The search range for the learning rate was set between 1×10^{-5} and 1×10^{-2}, and the number of neurons in the first dense layer was set between 32 and 128. The optimization was performed over 30 iterations, resulting in an improvement in validation accuracy from 90% to 94% compared to the baseline model.

3.7.3. Dataset Splitting and Validation

In this study, the data were split into 70% for training, 20% for validation, and 10% for testing to evaluate the model. The training data were used to train the model, while the validation data were used during training to prevent overfitting and assess the model's performance. Finally, the test data were used to validate the performance of the final model.

Additionally, 5-fold cross-validation was applied to ensure that every part of the dataset was used as validation data at least once, which helps prevent overfitting and reliably assesses the model's generalization performance. This validation technique is useful for evaluating the model's performance from multiple angles and ensuring that it is not biased toward a specific data split.

The study used various performance metrics such as MSE, MAE, SSIM, and ROC-AUC to evaluate the accuracy and generalization performance of the model. These metrics

played a crucial role in quantitatively assessing the model's ability to distinguish between normal and faulty data.

Table 4 presents the layer-wise configuration and parameter information of the CNN autoencoder-DNN combined model. The CNN autoencoder is designed to process the input data through multiple layers to extract key features, which are then combined with the DNN to perform fault diagnosis. The output shape and the number of parameters in each layer are important factors that determine the model's complexity.

Table 4. Layer configuration and parameter details of the CNN autoencoder and DNN model.

Model	Layer Name	Output Shape	Kernel Size/ Kernel Number/ Stride/ Zero-Padding	Number of Parameters
Raw Data CAE	conv2d	(None, 128, 3, 32)	(3, 3)/32/(1, 1)/same	320
	max_pooling2d	(None, 64, 2, 32)	(2, 2)/-/(2, 2)/same	0
	conv2d_1	(None, 64, 2, 64)	(3, 3)/64/(1, 1)/same	18,496
	max_pooling2d_1	(None, 32, 1, 64)	(2, 2)/-/(2, 2)/same	0
	conv2d_2	(None, 32, 1, 128)	(3, 3)/128/(1, 1)/same	73,856
	max_pooling2d_2	(None, 16, 1, 128)	(2, 2)/-/(2, 1)/same	0
	flatten	(None, 2048)	-	0
	encoded_layer (Dense)	(None, 32)	-	65,568
	dense (Dense)	(None, 2048)	-	67,584
	reshape	(None, 16, 1, 128)	-	0
	conv2d_3	(None, 16, 1, 128)	(3, 3)/128/(1, 1)/same	147,584
	up_sampling2d	(None, 32, 1, 128)	(2, 1)/-/(2, 1)/same	0
	conv2d_4	(None, 32, 1, 64)	(3, 3)/64/(1, 1)/same	73,792
	up_sampling2d_1	(None, 64, 1, 64)	(2, 1)/-/(2, 1)/same	0
	conv2d_5	(None, 64, 1, 32)	(3, 3)/32/(1, 1)/same	18,464
	up_sampling2d_2	(None, 128, 3, 32)	(2, 3)/-/(2, 3)/same	0
	conv2d_6	(None, 128, 3, 1)	(3, 3)/1/(1, 1)/same	289
Electrical System Data CAE	input_1	(None, 128, 3, 1)	-	0
	conv2d	(None, 128, 3, 16)	(3, 3)/16/(1, 1)/same	160
	max_pooling2d	(None, 64, 3, 16)	(2, 2)/-/(2, 2)/same	0
	conv2d_1	(None, 64, 3, 8)	(3, 3)/8/(1, 1)/same	1160
	max_pooling2d_1	(None, 32, 3, 8)	(2, 2)/-/(2, 2)/same	0
	flatten	(None, 768)	-	0
	encoded	(None, 32)	-	24,608
	dense	(None, 768)	-	25,344
	reshape	(None, 32, 3, 8)	-	0
	conv2d_transpose	(None, 64, 3, 8)	(3, 3)/8/(1, 1)/same	584
	conv2d_transpose_1	(None, 128, 3, 16)	(3, 3)/16/(1, 1)/same	1168
	conv2d_2	(None, 128, 3, 1)	(3, 3)/1/(1, 1)/same	145
Model	Layer Name	Output Shape	Activation Function	Number of parameters

Table 4. *Cont.*

Model	Layer Name	Output Shape	Kernel Size/ Kernel Number/ Stride/ Zero-Padding	Number of Parameters
Fault Diagnosis DNN	Dense_1	(None, 64)	ReLU	4160
	Dropout	(None, 64)	-	0
	Dense_3	(None, 32)	ReLU	2080
	Dropout_1	(None, 32)	-	0
	Output	(None, 2)	Softmax	66

4. Experiments and Results

4.1. Comparative Experiments (Model Performance Evaluation)

The performance of the proposed CNN autoencoder model is quantitatively evaluated through comparison with other machine learning techniques. This evaluation is based on performance metrics such as accuracy, recall, precision, and F1 score. The comparative experiments were conducted in two phases.

4.1.1. Experiment 1: Comparison with Conventional Machine Learning Models

The performance of the CNN autoencoder is compared and analyzed with conventional machine learning models such as SVM, decision tree, and random forest. The models are evaluated for bearing damage. The diagnostic sensitivity and specificity of each model are systematically measured using performance indicators including precision, recall, and F1 score, thereby verifying the detection accuracy of the proposed model.

4.1.2. Experiment 2: Performance Comparison with Other Deep Learning Models

The proposed CNN autoencoder model is evaluated against the latest deep learning techniques and CNN architectures. This comparison is based on performance metrics such as processing speed, accuracy, and recall.

4.2. Evaluation Metrics

Various metrics were used to evaluate the performance of the CNN autoencoder and DNN models. These metrics focus on comprehensively assessing the accuracy, generalization ability, and quality of the predictions of the models.

4.2.1. Mean Squared Error (MSE):

MSE (Mean Squared Error) calculates the average of the squared differences between predicted and actual values, making it sensitive to large errors. It is useful for capturing significant deviations in fault conditions and is effective in highlighting the differences between normal and fault data.

$$MSE = \frac{1}{n}\sum_{i=1}^{n}\left(Y_i - \hat{Y}_i\right)^2 \tag{18}$$

Here, Y_i is the actual value, and $\hat{Y}_i$ is the value predicted by the model.

4.2.2. Mean Absolute Error (MAE):

MAE (Mean Absolute Error) is calculated by averaging the absolute differences between the predicted and actual values. Unlike MSE, it is less sensitive to large errors, making it advantageous for evaluating overall predictive performance in a balanced manner. It is often used complementarily with MSE.

$$MAE = \frac{1}{n}\sum_{i=1}^{n}|Y_i - \hat{Y}_i| \tag{19}$$

4.2.3. Structural Similarity Index (SSIM):

SSIM (Structural Similarity Index Measure) is a metric used to evaluate the structural similarity between datasets by comprehensively analyzing three factors: luminance, contrast, and structure. It is useful for detecting structural differences between normal and fault data.

4.2.4. Peak Signal–Noise Ratio (PSNR):

PSNR (Peak Signal–Noise Ratio) is used to evaluate signal quality and is useful for detecting noise differences between normal and fault conditions. A higher PSNR value indicates better signal quality and less noise.

$$PSNR = 10 \cdot log_{10}\left(\frac{MSE_I^2}{MSE}\right) \tag{20}$$

4.2.5. Model Accuracy and Predictive Power Evaluation:

Accuracy indicates the proportion of correct predictions in the total data. Precision is the ratio of true positive predictions among positive predictions, and recall is the ratio of positive predictions among actual positives. The F1 score is the harmonic mean of precision and recall, which is useful for imbalanced datasets. The ROC-AUC Score (Receiver Operating Characteristic—Area Under Curve) evaluates the ability to distinguish between positive and negative classes, with performance closer to 1 being more desirable.

$$Accuracy = \frac{TP + TN}{TP + TN + FP + FN} \tag{21}$$

$$Precision = \frac{TP}{TP + FP} \tag{22}$$

$$Recall = \frac{TP}{TP + FN} \tag{23}$$

4.2.6. Interaction between MSE and PSNR

MSE and PSNR are complementary metrics used to evaluate model performance. MSE measures the average squared difference between predicted and actual values, with larger error sizes leading to higher MSE values. In contrast, PSNR decreases exponentially as the MSE increases, indicating that signal quality deteriorates as noise in the signal increases.

Additionally, SSIM and PSNR are used together in a complementary manner. While PSNR evaluates the overall quality of the signal, it may not capture the detailed structure of the data. For example, a high PSNR value may indicate a clean signal, but if the SSIM value is low, the structural consistency of the data may still be lacking. By using PSNR and SSIM in conjunction, both signal quality and structural integrity can be evaluated simultaneously.

In conclusion, MSE, PSNR, and SSIM each have distinct characteristics, and using them together provides a comprehensive approach to evaluating signal errors and data structure in motor fault diagnosis. The experimental results showed similar analysis outcomes for the three types of faults, so the graph for the bearing fault, which had the highest frequency and the most pronounced signal variations, was presented as the representative result.

Figure 14 shows the visualization of the high-dimensional data learned by the combined CAE and DNN model using PCA and t-SNE.PCA reduced the data to a two-dimensional space to visually distinguish between the normal and abnormal data, while t-SNE, a nonlinear dimensionality reduction technique, provided clearer clustering of the data. These visualization methods suggest that the model is capable of effectively distinguishing between normal and fault states.

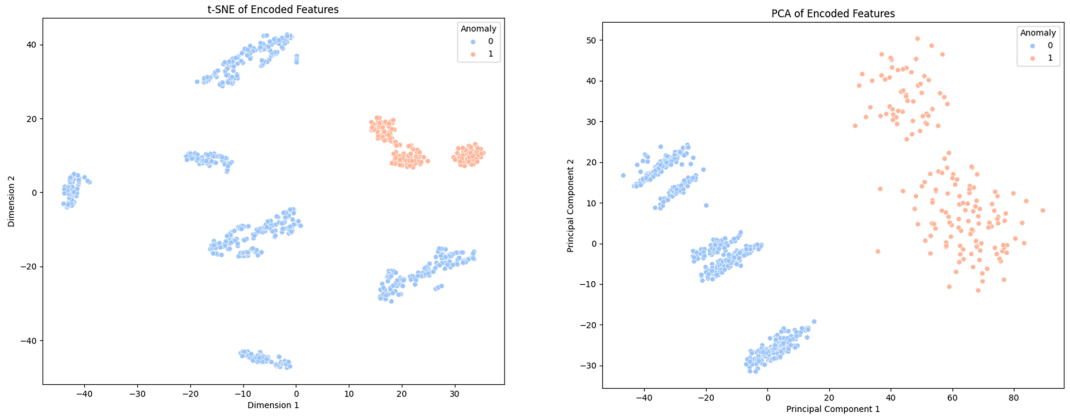

(**a**) (**b**)

Figure 14. Visualization of latent space using t-SNE and PCA: (**a**) the t-SNE of encoded features: the visualization of the latent space features extracted by the CAE model; (**b**) the PCA of encoded features: the projection of the feature vectors learned by the CAE model onto a 2D space using Principal Component Analysis (PCA).

The evaluation metrics used in the motor fault diagnosis paper play a crucial role in assessing the accuracy and quality of the data. Metrics such as Mean Absolute Error (MAE), Structural Similarity Index (SSIM), and Peak Signal–Noise Ratio (PSNR) are typically used in image analysis but can also be effectively applied in motor fault diagnosis.

In Figure 15a, changes in the Mean Squared Error (MSE) and Structural Similarity Index Measure (SSIM) observed in the training and validation data from the CAE using power system analysis data are shown. The rapid decrease in the MSE values for both the training and validation data indicates an improvement in the model's predictive accuracy. The SSIM value also reaches 0.98 as training progresses, indicating that the model maintains structural consistency in the data. MSE and SSIM complement each other, confirming that the model satisfies both quantitative accuracy and structural consistency.

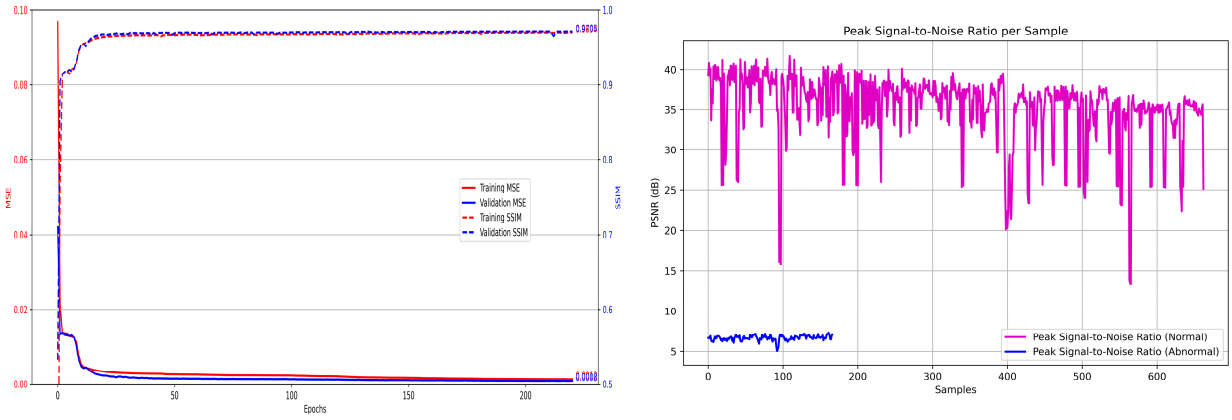

(**a**) (**b**)

Figure 15. Training and validation using CAE with power system analysis data: (**a**) epoch-wise changes in Mean Squared Error (MSE) and Structural Similarity Index (SSIM); (**b**) graph of Peak Signal–Noise Ratio (PSNR) changes for normal and abnormal samples.

In Figure 15b, the PSNR value of the normal samples remains stable between 35 dB and 40 dB, while the PSNR value of the abnormal samples drops to 5 dB to 10 dB, indicating a degradation in signal quality. The difference in signal quality between the two sample types suggests that PSNR is a useful metric for fault detection.

Figure 16a shows that the MSE loss value decreases rapidly in the early epochs and then stabilizes, indicating that the model has successfully learned the data patterns and

is delivering consistent performance without overfitting. In Figure 16b, the accuracy gradually increases over time, eventually achieving a high level of accuracy.

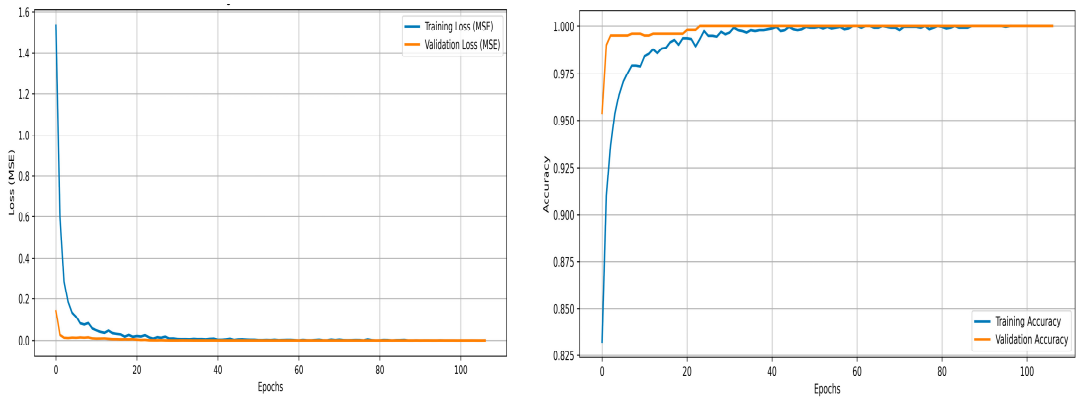

(**a**) (**b**)

Figure 16. Training and validation results in the DNN combined with raw data CAE and power system analysis data CAE: (**a**) the graph of MSE loss changes in the training and validation data of the combined DNN; (**b**) the graph of accuracy changes in the training and validation data.

In Figure 17a, the F1 score remains high for both training and validation, suggesting that the model accurately distinguishes between positive and negative classes, even with an imbalanced dataset. In Figure 17b, the ROC-AUC performance approaches a value close to 1, demonstrating the model's excellent performance in distinguishing between positive and negative classes.

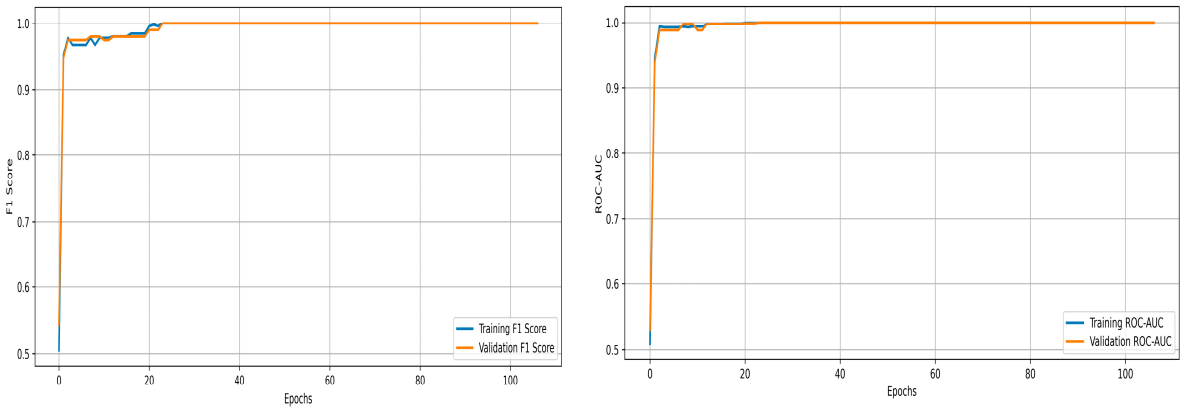

(**a**) (**b**)

Figure 17. (**a**) Changes in the F1 scores during the training and validation phases; (**b**) the graph of ROC-AUC performance across the training and validation epochs of the model.

4.3. Results and Analysis

In this study, the performance of the proposed CNN autoencoder-based model was evaluated by comparing it with traditional machine learning models (SVM, decision tree, and random forest) and deep learning models (DNN and CNN). Each model has a similar level of complexity, allowing us to confirm that performance differences are mainly due to the design of the models. Performance metrics such as accuracy, recall, precision, and F1 score were used for evaluation.

As shown in Table 5, the random forest model demonstrated superior performance compared to other machine learning models, but the proposed CNN-based model outperformed it.

Table 5. Comparison of machine learning model performance.

Model	Accuracy	Recall	Precision	F1 Score
SVM	85.5%	84.5%	86.0%	85.2%
Decision Tree	87.8%	87.1%	88.2%	87.6%
Random Forest	89.0%	88.5%	89.4%	88.9%

As shown in Tables 5 and 6, the SVM and decision tree models recorded accuracies of 85.5% and 87.8%, respectively, but their performance was unstable due to overfitting. The random forest model demonstrated excellent performance with 89.0% accuracy, but in real-time processing environments, its structural complexity could lead to reduced performance compared to the CNN model. While the DNN achieved 98.0% accuracy, excelling in learning nonlinear patterns, it was prone to overfitting. The CNN performed well with 98.6% accuracy but fell short compared to the proposed CNN autoencoder model. In contrast, the proposed model, which reflects the characteristics of power system analysis data, achieved an accuracy of 99.9%, recall of 99.8%, precision of 99.9%, and an F1 score of 99.9%. Thanks to its combined analytical structure with raw data, the proposed model exhibited superior performance in fault diagnosis.

Table 6. Comparison of deep learning model performance.

Model	Accuracy	Recall	Precision	F1 Score
DNN	98.0%	97.5%	98.4%	97.9%
CNN	98.6%	98.1%	98.7%	98.4%
Proposed Methodology	99.9%	99.8%	99.9%	99.9%

Although the proposed system delivers exceptional performance, environmental factors such as electrical noise, transient voltage, sound, and temperature fluctuations can negatively impact the accuracy of sensor signals, which could, in turn, reduce the model's diagnostic performance. To address these issues, various correction techniques were introduced. For instance, the 'DC Removal Filter' effectively eliminated electrical noise, and the 'sliding window' technique was employed to correct signal distortions caused by transient voltage. Additionally, the power system analyzer was used to monitor voltage and current data in real time, detecting abnormal signals, and the 'Z-score-based algorithm' was utilized to quickly assess data within the normal range. Signal distortions due to temperature changes were minimized by applying temperature compensation, helping to reduce signal distortion and maintain the model's diagnostic accuracy and reliability.

5. Conclusions

In this study, a high-performance fault diagnosis model was developed by combining a Convolutional Autoencoder (CAE) with a deep neural network (DNN) using power system analysis and electrical energy data. This model demonstrated excellent performance in learning nonlinear patterns and real-time data processing, significantly improving the speed and precision of fault detection compared to traditional diagnostic methods. By accurately analyzing voltage and current data to clearly distinguish between normal and abnormal patterns, the model can make an important contribution to motor management and the development of preventive maintenance strategies.

- Real-time Data Processing and the Effectiveness of Power System Analysis Data: The model processes data streams in real time, proving its practicality and effectiveness in industrial settings. The application of power system analysis data also validated the suitability of the CNN autoencoder.
- High-Performance Fault Diagnosis: The proposed model clearly distinguishes between normal and abnormal patterns by analyzing the voltage and current data of electric motors.

- Industrial Environment Application: The model is currently being applied in industrial settings, where it has proven real-time operation and received positive feedback.

Figure 18 shows the actual operational state of the mechanical press. The power system analysis equipment is installed in the distribution panel and collects electrical energy data from the R, S, and T phase power lines connected to the 110-ton and 80-ton motors.The model proposed in this study demonstrates its effectiveness in real-time fault diagnosis based on energy data generated from the power system, enhancing its practical utility and applicability in industrial environments. By contributing to the preventive maintenance of electrical equipment such as motor management and improving productivity, it is anticipated that this model can be generalized to a variety of motors due to the inherent electrical characteristics contained within the power system analysis data. However, further research is required to verify this generalizability, and confirming its applicability across diverse motor types will expand its potential for broader industrial adoption.

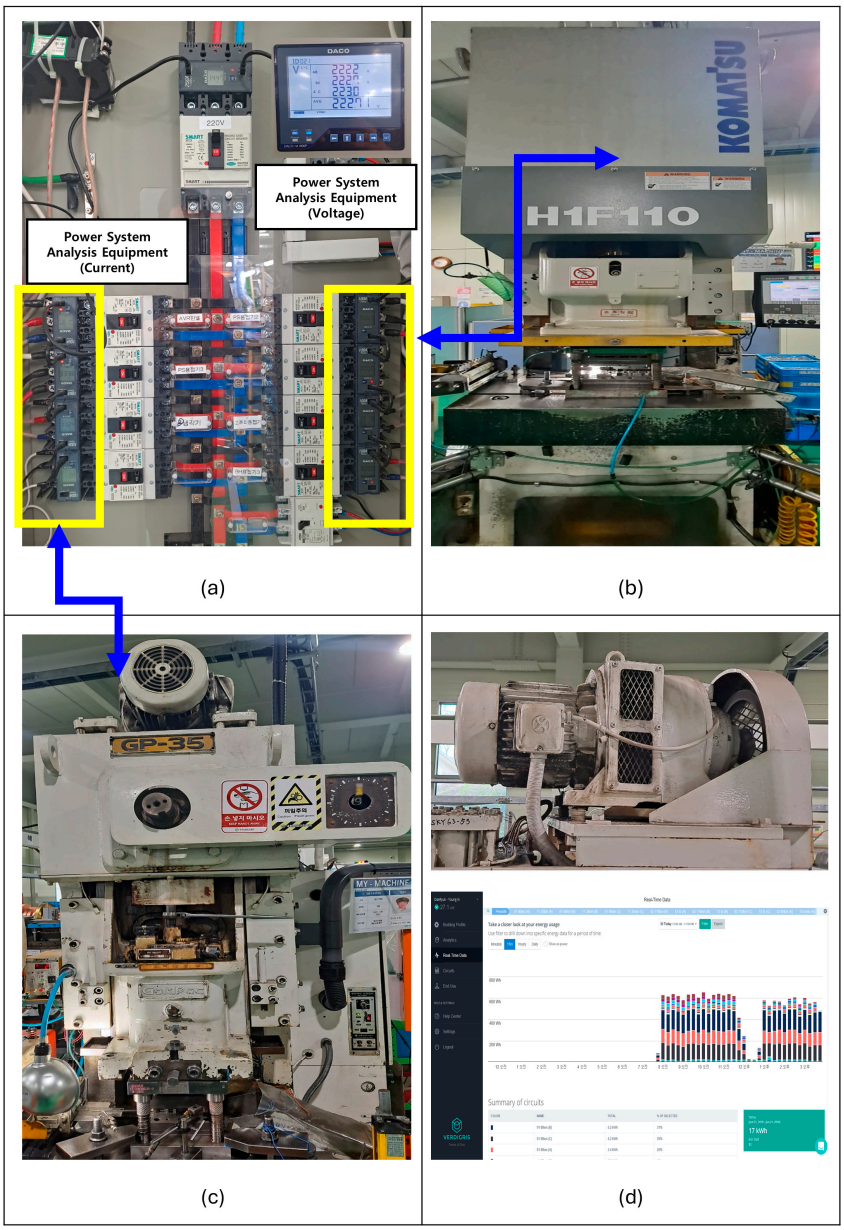

Figure 18. Analysis and operation equipment using CNN autoencoder and DNN combination for power system analysis: (**a**) voltage and current analysis system (power system analysis); (**b**) 110-ton mechanical press; (**c**) 80-ton mechanical press; (**d**) motor and real-time data monitoring software.

Future research should explore the following topics:

- Utilization of power system analysis data: Explore the possibility of effectively generalizing faults occurring under various electrical load conditions by mapping the R, S, and T phase electrical data to a CNN architecture.
- Model performance improvement: Apply data augmentation techniques to enhance the model's generalization performance across different fault types and operating conditions.
- Testing across various models and environments: Compare the performance with various machine learning models such as RNN, LSTM, and transformer to identify the optimal model.
- Research on electrical equipment faults and high-voltage arcs: Investigate the mechanisms of high-voltage arc occurrence and explore the application of technologies to detect these events.

Author Contributions: Conceptualization, Y.C. and I.J.; methodology, Y.C.; software, Y.C.; validation, I.J.; formal analysis, Y.C.; investigation, Y.C.; resources, I.J.; data curation, Y.C.; writing—original draft preparation, Y.C.; writing—review and editing, I.J.; visualization, Y.C.; supervision, I.J.; project administration, I.J. All authors have read and agreed to the published version of the manuscript.

Funding: This research received no external funding.

Data Availability Statement: The data that support the findings of this study are not available due to commercial restrictions.

Acknowledgments: The authors would like to thank the editor and the anonymous reviewers for their valuable comments and suggestions, which have significantly contributed to improving the quality of this manuscript.

Conflicts of Interest: The authors declare no conflicts of interest.

References

1. Gómez, J.R.; Sousa, V.; Eras, J.J.C.; Gutiérrez, A.S.; Viego, P.R.; Quispe, E.C.; de León, G. Assessment criteria of the feasibility of replacement standard efficiency electric motors with high-efficiency motors. *Energy* **2022**, *239*, 121877. [CrossRef]
2. Errigo, A.; Choi, J.K.; Kissock, K. Techno-economic-environmental impacts of industrial energy assessment: Sustainable industrial motor systems of small and medium-sized enterprises. *Sustain. Energy Technol. Assess.* **2022**, *49*, 101694. [CrossRef]
3. Cai, W.; Lai, K.H.; Liu, C.H.; Wei, F.F.; Ma, M.D.; Jia, S.; Jiang, Z.G.; Lv, L. Promoting sustainability of manufacturing industry through the lean energy-saving and emission-reduction strategy. *Sci. Total Environ.* **2019**, *665*, 23–32. [CrossRef] [PubMed]
4. de Souza, D.F.; da Guarda, E.L.A.; Sauer, I.L.; Tatizawa, H. Energy Efficiency Indicators for Water Pumping Systems in Multifamily Buildings. *Energies* **2021**, *14*, 7152. [CrossRef]
5. An, K.; Lu, J.F.; Zhu, Q.J.; Wang, X.X.; De Silva, C.W.; Xia, M.; Lu, S.L. Edge Solution for Real-Time Motor Fault Diagnosis Based on Efficient Convolutional Neural Network. *IEEE Trans. Instrum. Meas.* **2023**, *72*, 12. [CrossRef]
6. Song, X.J.; Wang, Z.W.; Hu, J.T. Detection of Bearing Outer Race Fault in Induction Motors using Motor Current Signature Analysis. In Proceedings of the 22nd International Conference on Electrical Machines and Systems (ICEMS), Harbin, China, 11–14 August 2019; pp. 2042–2046.
7. Kumar, R.R.; Andriollo, M.; Cirrincione, G.; Cirrincione, M.; Tortella, A. A Comprehensive Review of Conventional and Intelligence-Based Approaches for the Fault Diagnosis and Condition Monitoring of Induction Motors. *Energies* **2022**, *15*, 8938. [CrossRef]
8. Wu, H.; Ma, X.; Wen, C.L. Multilevel Fine Fault Diagnosis Method for Motors Based on Feature Extraction of Fractional Fourier Transform. *Sensors* **2022**, *22*, 1310. [CrossRef]
9. Langarica, S.; Rüffelmacher, C.; Núñez, F. An Industrial Internet Application for Real-Time Fault Diagnosis in Industrial Motors. *IEEE Trans. Autom. Sci. Eng.* **2020**, *17*, 284–295. [CrossRef]
10. Abid, A.; Khan, M.T.; Iqbal, J. A review on fault detection and diagnosis techniques: Basics and beyond. *Artif. Intell. Rev.* **2021**, *54*, 3639–3664. [CrossRef]
11. Akbar, S.; Vaimann, T.; Asad, B.; Kallaste, A.; Sardar, M.U.; Kudelina, K. State-of-the-Art Techniques for Fault Diagnosis in Electrical Machines: Advancements and Future Directions. *Energies* **2023**, *16*, 6345. [CrossRef]
12. Kafeel, A.; Aziz, S.; Awais, M.; Khan, M.A.; Afaq, K.; Idris, S.A.; Alshazly, H.; Mostafa, S.M. An Expert System for Rotating Machine Fault Detection Using Vibration Signal Analysis. *Sensors* **2021**, *21*, 7587. [CrossRef] [PubMed]
13. Toma, R.N.; Kim, J.M. Bearing Fault Classification of Induction Motors Using Discrete Wavelet Transform and Ensemble Machine Learning Algorithms. *Appl. Sci.* **2020**, *10*, 5251. [CrossRef]

14. Ventricci, L.; Ribeiro, R.F., Jr.; Gomes, G.F. Motor fault classification using hybrid short-time Fourier transform and wavelet transform with vibration signal and convolutional neural network. *J. Braz. Soc. Mech. Sci. Eng.* **2024**, *46*, 337. [CrossRef]
15. Qiu, S.H.; Cui, X.P.; Ping, Z.W.; Shan, N.L.; Li, Z.; Bao, X.Q.; Xu, X.H. Deep Learning Techniques in Intelligent Fault Diagnosis and Prognosis for Industrial Systems: A Review. *Sensors* **2023**, *23*, 1305. [CrossRef]
16. Li, Y.B.; Li, B.; Ji, J.C.; Kalhori, H. Advanced Fault Diagnosis and Health Monitoring Techniques for Complex Engineering Systems. *Sensors* **2022**, *22*, 10002. [CrossRef]
17. Hsu, C.Y.; Liu, W.C. Multiple time-series convolutional neural network for fault detection and diagnosis and empirical study in semiconductor manufacturing. *J. Intell. Manuf.* **2021**, *32*, 823–836. [CrossRef]
18. Wang, S.H.; Lei, Y.G.; Lu, N.; Li, X.; Yang, B. A multi-sensor relation model for recognizing and localizing faults of machines based on network analysis. *Front. Mech. Eng.* **2023**, *18*, 20. [CrossRef]
19. Carvalho, T.P.; Soares, F.; Vita, R.; Francisco, R.D.; Basto, J.P.; Alcalá, S.G.S. A systematic literature review of machine learning methods applied to predictive maintenance. *Comput. Ind. Eng.* **2019**, *137*, 106024. [CrossRef]
20. Bouabdallaoui, Y.; Lafhaj, Z.; Yim, P.; Ducoulombier, L.; Bennadji, B. Predictive Maintenance in Building Facilities: A Machine Learning-Based Approach. *Sensors* **2021**, *21*, 1044. [CrossRef]
21. Elkateb, S.; Métwalli, A.; Shendy, A.; Abu-Elanien, A.E.B. Machine learning and IoT-Based predictive maintenance approach for industrial applications. *Alex. Eng. J.* **2024**, *88*, 298–309. [CrossRef]
22. Jang, J.G.; Noh, C.M.; Kim, S.S.; Shin, S.C.; Lee, S.S.; Lee, J.C. Vibration data feature extraction and deep learning-based preprocessing method for highly accurate motor fault diagnosis. *J. Comput. Des. Eng.* **2023**, *10*, 204–220. [CrossRef]
23. Hamdaoui, H.; Ngiejungbwen, L.A.; Gu, J.A.; Tang, S.X. Improved signal processing for bearing fault diagnosis in noisy environments using signal denoising, time-frequency transform, and deep learning. *J. Braz. Soc. Mech. Sci. Eng.* **2023**, *45*, 576. [CrossRef]
24. Sawaqed, L.S.; Alrayes, A.M. Bearing fault diagnostic using machine learning algorithms. *Prog. Artif. Intell.* **2020**, *9*, 341–350. [CrossRef]
25. Zhou, H.T.; Chen, W.H.; Liu, J.; Cheng, L.S.; Xia, M. Trustworthy and intelligent fault diagnosis with effective denoising and evidential stacked GRU neural network. *J. Intell. Manuf.* **2023**, *35*, 3523–3542. [CrossRef]
26. Jia, W.K.; Sun, M.L.; Lian, J.; Hou, S.J. Feature dimensionality reduction: A review. *Complex Intell. Syst.* **2022**, *8*, 2663–2693. [CrossRef]
27. Sheng, Y.; Yan, J.D.; Piao, M.H. Improved wafer map defect pattern classification using automatic data augmentation based lightweight encoder network in contrastive learning. *J. Intell. Manuf.* **2024**, 1–3. [CrossRef]
28. Zou, X.; Zhang, H.M.; Jiang, Z.H.; Zhang, K.; Xu, Y.G. Toward accurate extraction of bearing fault modulation characteristics with novel time -frequency modulation bispectrum and modulation Gini index analysis. *Mech. Syst. Signal Process.* **2024**, *219*, 111629. [CrossRef]
29. Jiang, Z.H.; Zhang, K.; Xiang, L.; Yu, G.; Xu, Y.G. A time-frequency spectral amplitude modulation method and its applications in rolling bearing fault diagnosis. *Mech. Syst. Signal Process.* **2023**, *185*, 109832. [CrossRef]
30. Zhou, P.; Chen, S.Q.; He, Q.B.; Wang, D.; Peng, Z.K. Rotating machinery fault-induced vibration signal modulation effects: A review with mechanisms, extraction methods and applications for diagnosis. *Mech. Syst. Signal Process.* **2023**, *200*, 110489. [CrossRef]
31. Chen, X.H.; Zhang, B.K.; Gao, D. Bearing fault diagnosis base on multi-scale CNN and LSTM model. *J. Intell. Manuf.* **2021**, *32*, 971–987. [CrossRef]
32. Yin, Z.Y.; Zhang, F.Q.; Xu, G.Y.; Han, G.J.; Bi, Y.G. Multi-Scale Rolling Bearing Fault Diagnosis Method Based on Transfer Learning. *Appl. Sci.* **2024**, *14*, 1198. [CrossRef]
33. Gültekin, Ö.; Çinar, E.; Özkan, K.; Yazici, A. A novel deep learning approach for intelligent fault diagnosis applications based on time-frequency images. *Neural Comput. Appl.* **2022**, *34*, 4803–4812. [CrossRef]
34. Liu, J.Y.; Xie, F.Q.; Zhang, Q.; Lyu, Q.C.; Wang, X.S.; Wu, S.J. A multisensory time-frequency features fusion method for rotating machinery fault diagnosis under nonstationary case. *J. Intell. Manuf.* **2023**, *35*, 3197–3217. [CrossRef]
35. Du, Y.; Wang, A.M.; Wang, S.; He, B.M.; Meng, G.Y. Fault Diagnosis under Variable Working Conditions Based on STFT and Transfer Deep Residual Network. *Shock Vib.* **2020**, *2020*, 1274380. [CrossRef]
36. Pan, H.H.; Sun, W.C.; Sun, Q.M.; Gao, H.J. Deep Learning Based Data Fusion for Sensor Fault Diagnosis and Tolerance in Autonomous Vehicles. *Chin. J. Mech. Eng.* **2021**, *34*, 72. [CrossRef]
37. Huang, K.K.; Wu, S.J.; Li, Y.G.; Yang, C.H.; Gui, W.H. A multi-rate sampling data fusion method for fault diagnosis and its industrial applications. *J. Process. Control* **2021**, *104*, 54–61. [CrossRef]
38. Jin, T.S.; Zhang, C.X.; Zhang, Y.K.; Yang, M.L.; Ding, W.P. A Hybrid Fault Diagnosis Method for Autonomous Driving Sensing Systems Based on Information Complexity. *Electronics* **2024**, *13*, 354. [CrossRef]
39. Chuya-Sumba, J.; Alonso-Valerdi, L.M.; Ibarra-Zarate, D.I. Deep-Learning Method Based on 1D Convolutional Neural Network for Intelligent Fault Diagnosis of Rotating Machines. *Appl. Sci.* **2022**, *12*, 2158. [CrossRef]
40. Khorram, A.; Khalooei, M.; Rezghi, M. End-to-end CNN plus LSTM deep learning approach for bearing fault diagnosis. *Appl. Intell.* **2021**, *51*, 736–751. [CrossRef]
41. Principi, E.; Rossetti, D.; Squartini, S.; Piazza, F. Unsupervised Electric Motor Fault Detection by Using Deep Autoencoders. *IEEE-CAA J. Autom. Sin.* **2019**, *6*, 441–451. [CrossRef]

42. Lachekhab, F.; Benzaoui, M.; Tadjer, S.A.; Bensmaine, A.; Hamma, H. LSTM-Autoencoder Deep Learning Model for Anomaly Detection in Electric Motor. *Energies* **2024**, *17*, 2340. [CrossRef]
43. Orlowska-Kowalska, T.; Wolkiewicz, M.; Pietrzak, P.; Skowron, M.; Ewert, P.; Tarchala, G.; Krzysztofiak, M.; Kowalski, C.T. Fault Diagnosis and Fault-Tolerant Control of PMSM Drives-State of the Art and Future Challenges. *IEEE Access* **2022**, *10*, 59979–60024. [CrossRef]
44. Kim, Y.; Kim, Y.K. Time-Frequency Multi-Domain 1D Convolutional Neural Network with Channel-Spatial Attention for Noise-Robust Bearing Fault Diagnosis. *Sensors* **2023**, *23*, 9311. [CrossRef] [PubMed]
45. Al Mamun, A.; Bappy, M.M.; Mudiyanselage, A.S.; Li, J.L.; Jiang, Z.P.; Tian, Z.H.; Fuller, S.; Falls, T.C.; Bian, L.K.; Tian, W.M. Multi-channel sensor fusion for real-time bearing fault diagnosis by frequency-domain multilinear principal component analysis. *Int. J. Adv. Manuf. Technol.* **2023**, *124*, 1321–1334. [CrossRef]
46. Qian, L.; Li, B.B.; Chen, L.J. CNN-Based Feature Fusion Motor Fault Diagnosis. *Electronics* **2022**, *11*, 2746. [CrossRef]
47. Sonmez, E.; Kacar, S.; Uzun, S. A new deep learning model combining CNN for engine fault diagnosis. *J. Braz. Soc. Mech. Sci. Eng.* **2023**, *45*, 644. [CrossRef]
48. Cai, B.P.; Hao, K.K.; Wang, Z.; Yang, C.; Kong, X.D.; Liu, Z.K.; Ji, R.J.; Liu, Y.H. Data-driven early fault diagnostic methodology of permanent magnet synchronous motor. *Expert Syst. Appl.* **2021**, *177*, 115000. [CrossRef]
49. Souza, R.M.; Nascimento, E.G.S.; Miranda, U.A.; Silva, W.J.D.; Lepikson, H.A. Deep learning for diagnosis and classification of faults in industrial rotating machinery. *Comput. Ind. Eng.* **2021**, *153*, 107060. [CrossRef]
50. Tao, H.F.; Qiu, J.R.; Chen, Y.Y.; Stojanovic, V.; Cheng, L. Unsupervised cross-domain rolling bearing fault diagnosis based on time-frequency information fusion. *J. Frankl. Inst.-Eng. Appl. Math.* **2023**, *360*, 1454–1477. [CrossRef]
51. Wang, H.; Liu, Z.L.; Peng, D.D.; Yang, M.; Qin, Y. Feature-Level Attention-Guided Multitask CNN for Fault Diagnosis and Working Conditions Identification of Rolling Bearing. *IEEE Trans. Neural Netw. Learn. Syst.* **2022**, *33*, 4757–4769. [CrossRef]
52. Zhao, H.M.; Liu, J.; Chen, H.Y.; Chen, J.; Li, Y.; Xu, J.J.; Deng, W. Intelligent Diagnosis Using Continuous Wavelet Transform and Gauss Convolutional Deep Belief Network. *IEEE Trans. Reliab.* **2023**, *72*, 692–702. [CrossRef]
53. Gundewar, S.K.; Kane, P.V. Condition Monitoring and Fault Diagnosis of Induction Motor. *J. Vib. Eng. Technol.* **2021**, *9*, 643–674. [CrossRef]
54. Gyftakis, K.N.; Cardoso, A.J.M. Reliable Detection of Stator Interturn Faults of Very Low Severity Level in Induction Motors. *IEEE Trans. Ind. Electron.* **2021**, *68*, 3475–3484. [CrossRef]
55. Pham, M.T.; Kim, J.M.; Kim, C.H. Accurate Bearing Fault Diagnosis under Variable Shaft Speed using Convolutional Neural Networks and Vibration Spectrogram. *Appl. Sci.* **2020**, *10*, 6385. [CrossRef]
56. Roy, S.S.; Dey, S.; Chatterjee, S. Autocorrelation Aided Random Forest Classifier-Based Bearing Fault Detection Framework. *IEEE Sens. J.* **2020**, *20*, 10792–10800. [CrossRef]
57. Skowron, M.; Orlowska-Kowalska, T.; Wolkiewicz, M.; Kowalski, C.T. Convolutional Neural Network-Based Stator Current Data-Driven Incipient Stator Fault Diagnosis of Inverter-Fed Induction Motor. *Energies* **2020**, *13*, 1475. [CrossRef]
58. Shao, S.Y.; Yan, R.Q.; Lu, Y.D.; Wang, P.; Gao, R.X. DCNN-Based Multi-Signal Induction Motor Fault Diagnosis. *IEEE Trans. Instrum. Meas.* **2020**, *69*, 2658–2669. [CrossRef]
59. Zhang, S.; Zhang, S.B.; Wang, B.N.; Habetler, T.G. Deep Learning Algorithms for Bearing Fault Diagnostics—A Review. In Proceedings of the 12th IEEE International Symposium on Diagnostics for Electrical Machines, Power Electronics and Drives (SDEMPED), Toulouse, France, 27–30 August 2019; pp. 257–263.
60. Prosvirin, A.E.; Ahmad, Z.; Kim, J.M. Global and Local Feature Extraction Using a Convolutional Autoencoder and Neural Networks for Diagnosing Centrifugal Pump Mechanical Faults. *IEEE Access* **2021**, *9*, 65838–65854. [CrossRef]
61. Yu, J.B.; Zhou, X.K. One-Dimensional Residual Convolutional Autoencoder Based Feature Learning for Gearbox Fault Diagnosis. *IEEE Trans. Ind. Inform.* **2020**, *16*, 6347–6358. [CrossRef]
62. Liang, X.D.; Ali, M.Z.; Zhang, H.G. Induction Motors Fault Diagnosis Using Finite Element Method: A Review. *IEEE Trans. Ind. Appl.* **2020**, *56*, 1205–1217. [CrossRef]
63. Adekitan, A.I. A New Definition of Voltage Unbalance Using Supply Phase Shift. *J. Control Autom. Electr. Syst.* **2020**, *31*, 718–725. [CrossRef]
64. Suresh, V.; Janik, P.; Rezmer, J.; Leonowicz, Z. Forecasting Solar PV Output Using Convolutional Neural Networks with a Sliding Window Algorithm. *Energies* **2020**, *13*, 723. [CrossRef]
65. Huang, T.; Zhang, Q.; Tang, X.A.; Zhao, S.Y.; Lu, X.N. A novel fault diagnosis method based on CNN and LSTM and its application in fault diagnosis for complex systems. *Artif. Intell. Rev.* **2022**, *55*, 1289–1315. [CrossRef]